Journal of Biomolecular NMR (2005) 31: 311–320
DOI 10.1007/s10858-005-1605-7
© Springer 2005

Article

Dynamics in the cyclic Enterobacterial common antigen as studied by ^{13}C NMR relaxation

August Andersson[a], Åsa Ahl[a], Robert Eklund[b], Göran Widmalm[b] & Lena Mäler[a,*]
[a]*Department of Biochemistry and Biophysics, Arrhenius Laboratory, Stockholm University, 106 91, Stockholm, Sweden;* [b]*Department of Organic Chemistry, Arrhenius Laboratory, Stockholm University, 106 91, Stockholm, Sweden*

Received 27 October 2004; Accepted 21 January 2005

Key words: anisotropy, carbohydrate, dynamics, ECA, NMR, relaxation

Abstract

The motional properties of the cyclic enterobacterial common antigen (cECA), consisting of four trisaccharide repeat units, have been investigated by carbon-13 spin relaxation. R_1, R_2 and NOE relaxation parameters have been determined at three magnetic field strengths. The data were interpreted within the model-free framework to include the possibility of motional anisotropy, and overall as well as local dynamical parameters were fitted separately for each ring carbon. The motional anisotropy was addressed by assuming an axially symmetric diffusion tensor, which was fitted from the overall correlation times for each site in the sugar residues using the previously determined crystal structure. The data were found to be in agreement with an oblate shape of the molecule, and the values for D_{iso} and $D_{\|}/D_{\perp}$ were in good agreement with translational diffusion data and an estimate based on calculation of the moment of inertia tensor, respectively. The local dynamics in cECA were found to be residue-dependent. Somewhat lower values for the order parameters, as well as longer local correlation times, were observed for the β-linked ManNAcA residue compared to the two α-linked residues in the trisaccharide repeat unit.

Introduction

Polysaccharides constitute an important part at the surface of bacteria. In Gram-positive bacteria the outer cell-wall is built of peptidoglycans and the bacterium is surrounded by a type specific capsular polysaccharide (CPS). In addition, in some species a common polysaccharide is present, e.g., in pneumococci it is referred to as the C-polysaccharide (Karlsson et al., 1999) and has a complex and distinctly different structure compared to those of each type specific strain. In Gram-negative bacteria the outer membrane (Beveridge, 1999) has lipopolysaccharides (LPS) anchored to it with $\sim 10^6$ LPS molecules per cell. These bacteria may also have a CPS coat. The genus Enterobacteriaceae has the enterobacterial common antigen (Kuhn et al., 1988), which consists of trisaccharide repeating units with the structure: $\rightarrow$ 3)-α-D-Fuc*p*4NAc-(1 $\rightarrow$ 4)-β-D-Man*p*NAcA-(1 $\rightarrow$ 4)-α-D-Glc*p*NAc-(1 $\rightarrow$, in shorthand denoted FMG with respect to the constituent sugar residues. Two of the three aminosugars, i.e., residues F and M, are rather unusual as components of bacterial polysaccharides. Most interestingly, this polymerized trisaccharide repeat is found in different forms, namely, (i) as a phosphoglyceride linked component, (ii) attached via a core region to a Lipid A carrier thus forming an LPS, and (iii) in a cyclic form with four (Figure 1) to six repeating units. The cyclic form with four repeating units

*To whom correspondence should be addressed. E-mail: lena.maler@dbb.su.se

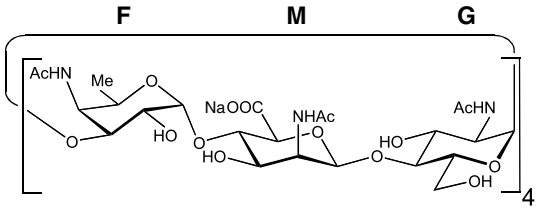

Figure 1. Schematic of the cECA dodecasaccharide (cECA) having a repeating unit of → 3)-α-D-Fuc*p*4NAc-(1 → 4)-β-D-Man*p*NAcA-(1 → 4)-α-D-Glc*p*NAc-(1 → .

(cECA) has been characterized in different species such as *Yersinia pestis* (Vinogradov et al., 1994), *Plesiomonas shigelloides* (Staaf et al., 2001) and *Escherichia coli* (Erbel et al., 2003).

Our previous conformational analysis of cyclic enterobacterial common antigen (cECA) in solution was based on NMR $^{1}H,^{1}H$ NOEs, $^{1}H,^{13}C$ trans-glycosidic scalar coupling constants and $^{1}H,^{13}C$ residual dipolar couplings in conjunction with molecular dynamics simulations (Staaf et al., 2001). The simulations suggested that more than one well-defined conformational state could be present at the M to G glycosidic linkage. Subsequently, we were able to determine the crystal structure of cECA, which crystallized in two distinct conformations (Färnbäck et al., 2003). One adopts an almost perfect square structure, while the other adopts a slightly tilted rhombic structure (Figure 2). In the solid-state investigation, conformational differences between the two structures were seen at the F to M glycosidic linkage. Thus, both studies indicate that the conformational preferences for cECA are intricate. As a result of this we have now turned to ^{13}C NMR relaxation studies, which can reveal information on short time-scale dynamics, in the ps to ns time regime, as well as processes on the μs to ms time scale.

One problem with the analysis of relaxation parameters in terms of molecular dynamics is the possibility of motional anisotropy as well as conformational exchange phenomena taking place on a time-scale which influences the measured R_2 relaxation rates. For non-spherical, or non-globular molecules, such as most carbohydrates the issue of rotational diffusion anisotropy may become very important. Rotational diffusion anisotropy has important implications in nuclear spin relaxation (Woessner, 1962). Separating internal dynamics from motional anisotropy needs to be carefully addressed. This issue has previously been discussed for a linear pentasaccharide (Rundlöf et al., 1999). As cECA is evidently non-spherical, the anisotropy of tumbling is herein also addressed. In this study we report on multiple-field ^{13}C relaxation and the

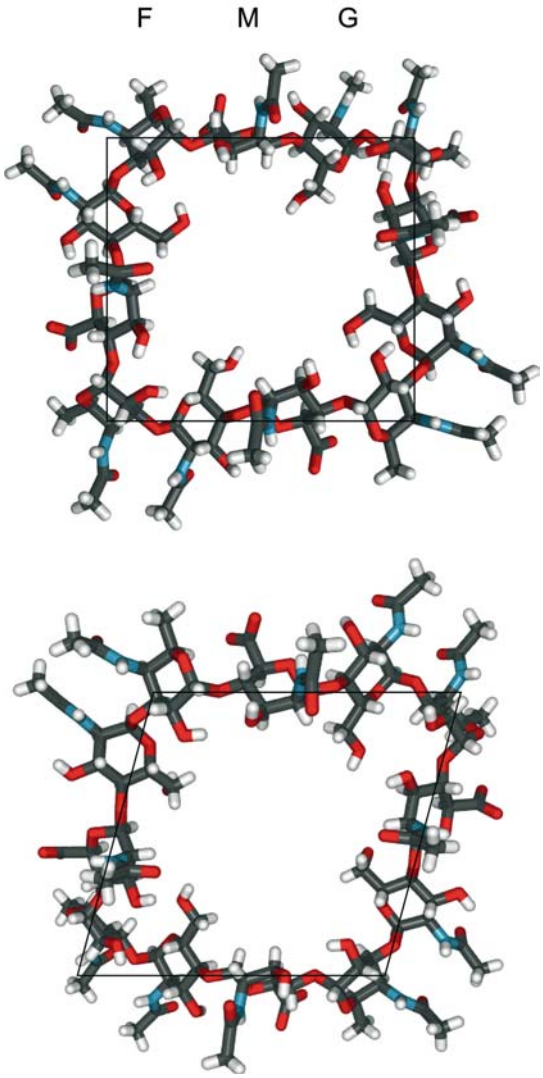

Figure 2. The two crystal forms of cECA. The top panel shows the square and the lower panel shows the rhombic structure. Coordinates were taken from Färnbäck et al. (2003).

interpretation in terms of overall and local dynamics. The results can be related to the previous structural investigations of cECA, and we comment on the possibility of conformational exchange dynamics and evaluate site-specific dynamic parameters.

Experimental

Sample preparation

The lipopolysaccharide from a *Plesiomonas shigelloides* strain (Staaf et al., 2001) was delipidated with 0.1 M NaOAc pH 4.2, 100 °C for 4 h and the solution was neutralized with 4 M NaOH. The solution was centrifuged and the supernatant was dialyzed for 60 h using Spectra Por, 4 MWCO 12–14,000. It was filtered and the material was separated on an anion exchange column, DEAE Sepharose, fast flow. The oligosaccharide (cECA) was then purified from the polysaccharide using gel permeation chromatography on a Superdex-30 column connected to an Fast Performance Liquid Chromatography (FPLC) system, where the material eluted after the void volume. For NMR experiments in solution, cECA (1.9 mg) was dissolved in 300 μl D_2O to give a concentration of 2.6 mM and the pH was adjusted to 8.5.

NMR spectroscopy

NMR experiments were carried out on Bruker Avance spectrometers operating at 9.39 and 11.75 T, as well as on a Varian Inova spectrometer operating at 18.78 T. The temperature was set to 293 K, and the temperature was calibrated using a thermocouple, which was inserted into a regular NMR tube containing H_2O. Two-dimensional ^1H,^1H COSY (Aue et al., 1976), TOCSY (Braunschweiler and Ernst, 1983) and NOESY (Jeener et al., 1979) experiments were recorded at 400 MHz, using an excitation sculpting sequence for suppressing the residual water signal (Hwang and Shaka, 1995). The homonuclear data were recorded as 2048×512 complex points matrices, using the States-TPPI method. The relaxation measurements were carried out at natural abundance of ^{13}C. Two-dimensional indirect-detected ^{13}C relaxation data were recorded (Skelton et al., 1993) as data sets typically consisting of 2048×128 complex points, using 32–48 transients for each FID (32–48 h total recording time for each relaxation measurement series). R_1 relaxation rates were measured at 9.39, 11.75 and 18.78 T while R_2 relaxation rates were measured at 11.75 and 18.78 T. Steady-state NOE factors were measured at 9.39 and 18.78 T. The R_1 and R_2 relaxation rates were obtained from a minimum of 11 time delays, and two time points were recorded at least twice for error analysis. Relaxation delays ranging between 0 and 2 s were used in the R_1 measurements, while delays ranging between 0 and 0.3 s were used in the R_2 measurements. The R_1 and R_2 relaxation rates were evaluated by a non-linear three-parameter fit. Heteronuclear NOE was measured by taking the ratio of peak volumes from spectra recorded interleaved with and without ^1H broad-band decoupling prior to the pulse sequence. The decoupling was turned on for a duration of 5 s and a corresponding minimum pre-acquisition delay of 5 s was used in the NOE experiments. The NOE experiments were recorded at least twice for error analysis. A conservative error estimate was however used for the NOE data, and no errors were set to lower than 5%.

Translational diffusion experiments for cECA were recorded at 298 K and 500 MHz ^1H frequency, with a Bruker Avance spectrometer equipped with a cryoprobe, using the modified Stejskal–Tanner spin echo experiments with a gradient pre-pulse (Stejskal and Tanner, 1965; von Meerwall and Kamat, 1989; Callaghan et al., 1998). The diffusion measurements were carried out using fixed time intervals linearly incremented up to the maximum power level of $\sim$22 G/cm. The T_1-delay was set to 0.05 s. The accuracy in the diffusion measurements was improved by correcting for non-linear gradients according to Damberg et al. (2001).

Relaxation data evaluation

The ^{13}C relaxation data was evaluated by using the model-free approach by Lipari and Szabo (1982). For an isolated ^{13}C–^1H pair, which can be assumed for natural abundance ^{13}C, the relaxation is dominated by the dipole–dipole interaction between the two nuclei. The relaxation rates are given by:

$$R_1 = \frac{1}{4}d^2[J(\omega_H - \omega_C) + 3J(\omega_C) + 6J(\omega_H + \omega_C)] + c^2 J(\omega_C) \quad (1)$$

$$R_2 = \frac{1}{8}d^2[4J(0) + J(\omega_H - \omega_C) + 3J(\omega_C) + 6J(\omega_H + \omega_C)] + \frac{1}{6}c^2[3J(\omega_C) + 4J(0)] \quad (2)$$

$$NOE = 1 + \frac{d^2\gamma_H}{4R_1\gamma_C}(6J(\omega_H + \omega_C) - J(\omega_H - \omega_C)) \quad (3)$$

in which d is the dipole–dipole interaction strength constant given by $d = (\mu_0/4\pi)\gamma_H\gamma_C\hbar r_{CH}^{-3}$ and c is the CSA interaction strength constant given by $c = (1/\sqrt{3})\gamma_C B_0 \Delta\sigma$. r_{CH} is the internuclear distance, set to 1.09 Å, and $\Delta\sigma$ is the CSA, assumed to be axially symmetric. A value of $\Delta\sigma = 25$ ppm was used in the analysis (Cavanagh et al., 1996; Wei et al., 2001).

The data were fitted to the model-free spectral density using the program Modelfree (version 4.01, Palmer et al., 1991; Mandel et al., 1995). In this model the data are fitted to the spectral density function given by

$$J(\omega) = \frac{2}{5}\left[\frac{S^2\tau_{loc}}{1 + \omega^2\tau_{loc}^2} + \frac{(1 - S^2)\tau}{1 + \omega^2\tau^2}\right] \quad (4)$$

in which S is the generalized order parameter, τ_{loc} is the global overall correlation time for each site in the molecule, $\tau = \tau_{loc}^{-1} + \tau_e^{-1}$, and τ_e is the local correlation for each site. Assuming an axially symmetric diffusion tensor, the expression for the spectral density function becomes

$$J(\omega) = \sum_{j=0}^{2} A_j\left[S^2\frac{\tau_j}{1 + \omega^2\tau_j^2} + (1 - S^2)\frac{\tau_j'}{1 + \omega^2\tau_j'^2}\right] \quad (5)$$

in which $\tau_j^{-1} = 6D_\perp - j^2(D_\perp - D_\parallel)$, $D_\perp$ and $D_\parallel$ are principal components of the axially symmetric diffusion tensor, and the coefficients A_j are functions of the angle θ between the principal axes of the the internuclear vector and the unique axis of the diffusion tensor, $A_0 = (1.5\cos^2\theta - 0.5)^2$, $A_1 = 3\sin^2\theta\cos^2\theta$, $A_2 = 0.75\sin^4\theta$. Finally, $1/\tau_j' = 1/\tau_j + 1/\tau_e$, where τ_e is the correlation time for the internal motion of the internuclear vector, in analogy with the spectral density function for the isotropic case.

In order for the model to be valid the global correlation time has to be common to the entire molecule. The data were however fitted individually for each site, using Equation 4, thus obtaining a local global correlation time for each ^{13}C nucleus within the residues, as indicated by Equation 4. The diffusion tensor can alternatively be found by using the approach by Brüschweiler et al. (1995) who demonstrated that for small diffusion anisotropies, the local diffusion constant D_i for the i:th bond vector for a symmetric top can be written as

$$D_i = (D_\parallel + D_\perp)/2 + (D_\perp - D_\parallel)(a_{31}x_i + a_{32}y_i + a_{33}z_i)^2/2 \quad (6)$$

where $a_{31} = \sin\theta\cos\phi$, $a_{32} = \sin\theta\sin\phi$ and $a_{33} = \cos\theta$. The angles θ and ϕ define the orientation of the symmetry axis of the axially symmetric diffusion tensor. The parameters $D_\parallel$, $D_\perp$, θ and ϕ can be found by least-squares optimization. The local correlation times obtained from the model-free approach were in this way evaluated in terms of global motional anisotropy using the program Quadric Diffusion (Lee et al., 1997). An X-ray structure determination of cECA has been performed (Färnbäck et al., 2003) and the available structures were used in evaluating the global correlation times in terms of motional anisotropy.

Results

A combination of two-dimensional (2D) homonuclear NMR experiments was used to verify the ^{1}H resonance assignments for cECA (Erbel et al., 2003). Due to overlap in the ^{13}C spectrum of cECA, relaxation data were recorded as 2D indirect detected experiments. Relaxation data was obtained for the cyclic form of the Enterobacterial common antigen (cECA) for all carbon positions in the molecule, except one (F–C3), and the data are collected in Table 1. cECA consists of the tetra-repeat → 3)-α-D-Fuc*p*4NAc-(1 → 4)-β-D-Man*p*NAcA-(1 → 4)-α-D-Glc*p*NAc-(1 → , where

Fuc4Nac, ManNAcA, and GlcNAc denote 4-acetamido-4,6-dideoxy-D-galactose, *N*-acetyl-D-mannosaminuronic acid, and *N*-acetyl-D-glucosamine, respectively (Figure 1). The ^{13}C NMR spectrum for the ring carbons consists of 15 resonances, corresponding to one repeat unit. Thus, the four repeats are seen to be equivalent. Furthermore, the structure of ECA has previously been determined by X-ray crystallography (Figure 2), which showed that cECA crystallizes in two distinct forms, a square and a rhombic structure. In the NMR data, we see no evidence of two different conformations unless they are in fast exchange, since only one set of resonances was observed.

Prior to the relaxation investigation we obtained an estimate of the global correlation time of the molecule using the well-known Stokes–Einstein relationship. The translational diffusion coefficient for cECA was found to be $D_t = 1.65 \times 10^{-10}$ m^2 s^{-1} at 298 K, which results in a global correlation time $\tau_m = 2.3$ ns at 293 K, assuming a spherical object. This approximation is crude, since assumptions on the shape of the molecule makes estimates of global rotational motion difficult (Chou et al., 2004), but nevertheless provides an estimate of the global reorientational correlation time. One can however include the effect of the shape of the molecule. Hydrodynamic considerations of the moment of inertia tensor using arguments about hydration as discussed by Rundlöf et al. (1999) were performed in order to compare with the diffusion results and with the motional parameters obtained from relaxation. For the rhombic structure, the principal components of the tensor were found to be $I_{xx} = 1$, $I_{yy} = 1.26$ and $I_{zz} = 2.08$. As expected a more axially symmetric moment of inertia tensor is found for the square structure with $I_{xx} = 1$, $I_{yy} = 1.12$ and $I_{zz} = 1.96$. Using these values, the difference in correlation time for a spherical object and an oblate one, given by the difference in the Perrin shape parameter (Cantor and Shimmel, 1980), is only a factor of 1.03.

In order to further elucidate the motional behavior of cECA we measured R_1, R_2 and steady-state relaxation parameters at three fields. The relaxation data are collected in Table 1. Due to spectral overlap no reliable data could be obtained for the C3–H3 spin-pair in residue F and consequently no evaluation in terms of dynamics was made. The data were interpreted with the model-free approach using the Modelfree software (Mandel et al., 1995). A model-selection was made according to Mandel et al. (1995) and it was found that no phenomenological exchange term was needed to fit the R_2 data, indicating that no conformational exchange between two conformers is present. An exchange between a conformation with a relatively small population (a few percent) and a larger one would, however, be difficult to

Table 1. Carbon-13 relaxation data for cECA at 293 K obtained at three magnetic field strengths.

Carbon[a]	9.39 T		11.75 T			18.78 T	
	R_1 (s^{-1})	NOE	R_1 (s^{-1})	R_2 (s^{-1})	NOE	R_1 (s^{-1})	R_2 (s^{-1})
F–C1	5.13 ± 0.25	1.44 ± 0.07	3.93 ± 0.19	11.96 ± 0.55	1.34 ± 0.06	1.77 ± 0.08	8.03 ± 0.40
F–C2	4.18 ± 0.20	1.44 ± 0.07	3.67 ± 0.18	9.12 ± 0.45	1.43 ± 0.07	1.69 ± 0.08	8.09 ± 0.40
F–C4	4.92 ± 0.24	1.35 ± 0.06	3.94 ± 0.19	14.73 ± 0.70	1.35 ± 0.06	1.78 ± 0.09	8.17 ± 0.41
F–C5	4.58 ± 0.23	1.37 ± 0.06	3.81 ± 0.19	10.12 ± 0.50	1.34 ± 0.05	1.77 ± 0.08	8.46 ± 0.40
M–C1	4.52 ± 0.23	1.55 ± 0.06	3.72 ± 0.18	n.d.[b]	1.47 ± 0.07	1.86 ± 0.09	7.73 ± 0.39
M–C2	4.46 ± 0.22	1.48 ± 0.07	3.80 ± 0.19	11.35 ± 0.50	1.48 ± 0.07	1.75 ± 0.09	8.38 ± 0.41
M–C3	4.48 ± 0.24	1.46 ± 0.07	3.59 ± 0.10	7.79 ± 0.39	1.45 ± 0.07	1.80 ± 0.09	6.48 ± 0.29
M–C4	3.89 ± 0.19	1.63 ± 0.08	3.82 ± 0.19	10.37 ± 0.50	1.40 ± 0.07	1.82 ± 0.09	8.20 ± 0.41
M–C5	4.39 ± 0.22	1.20 ± 0.06	3.63 ± 0.18	8.70 ± 0.44	1.48 ± 0.07	1.82 ± 0.09	6.82 ± 0.34
G–C1	4.91 ± 0.25	1.31 ± 0.06	3.85 ± 0.15	9.73 ± 0.40	1.34 ± 0.05	1.84 ± 0.09	7.77 ± 0.30
G–C2	4.55 ± 0.20	1.39 ± 0.05	3.78 ± 0.14	10.15 ± 0.70	1.37 ± 0.07	2.07 ± 0.10	7.97 ± 0.30
G–C3	4.72 ± 0.20	1.30 ± 0.06	4.09 ± 0.20	8.41 ± 0.40	1.37 ± 0.07	1.82 ± 0.08	8.18 ± 0.40
G–C4	4.78 ± 0.20	1.51 ± 0.08	4.09 ± 0.20	9.52 ± 0.40	1.42 ± 0.07	1.89 ± 0.08	8.33 ± 0.40
G–C5	4.33 ± 0.22	1.28 ± 0.07	3.78 ± 0.15	8.72 ± 0.44	1.36 ± 0.07	1.69 ± 0.09	7.66 ± 0.38

[a]Relaxation parameters were not measured for F–C3. [b]Not determined.

detect, since we do not expect large chemical shift differences between the two states. Assuming an exchange rate on the order of 1 ms, the apparent difference in R_2 would be on the order of the errors in the measurement. Nevertheless, we see no evidence of conformational exchange on this time-scale influencing our R_2 relaxation rates, i.e., on the μs to ms time-scale. One can note, however, that an exchange process on the same time-scale as the overall global motion would result in an influence on the apparent overall global correlation time, and the two cannot be separated. An exchange process on a somewhat slower time-scale could in principle be detected through introducing a model similar to the extended model-free spectral density function allowing for two separate internal motions (Clore et al., 1990), but we see no improvement in the fit when using such a model.

The absence of exchange is evident already from observation of the R_2 data (Table 1) in which a decrease in R_2 with magnetic field strength is seen for all carbons. The presence of chemical exchange would have the effect of increasing the apparent R_2 relaxation rate. More specifically, the quantity $\Delta = R_2 - R_1/2$ should increase with the square of the magnetic field (Phan et al., 1996). The R_2/R_1 ratio (Figure 3) carries information about the local variability in either overall global reorientation, i.e., anisotropy, or in chemical exchange. Since no exchange term was needed to fit the data, the variability in the R_2/R_1 ratio indicates motional anisotropy. Consequently the data were finally interpreted with a model consisting of a local global correlation time for each C–H bond vector, a generalized order parameter squared and a local correlation time for the internal motion for each site in the molecule, using

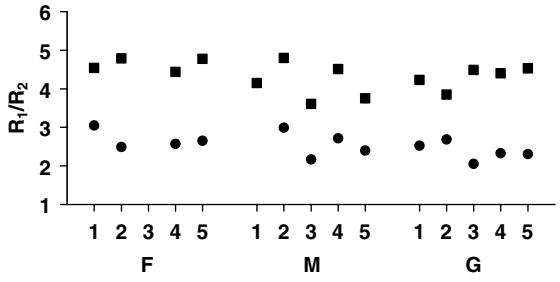

Figure 3. R_2/R_1 Relaxation rate ratios for cECA at 293 K. Circles indicate R_2/R_1 ratios at 11.75 T and squares indicate ratios obtained at 18.78 T.

Equation 4. The experimental relaxation rates for the anomeric carbons in each residue together with the calculated relaxation rates from the derived motional parameters are shown in Figure 4. The local overall correlation times were indeed found to vary, and therefore the question of motional anisotropy was addressed. cECA crystallizes in two distinct forms, one close to a square geometry and a second in a rhombic form. The local correlation times were used together with the X-ray structures of cECA to calculate the diffusion tensor using an axially symmetric diffusion model. The two structures were used to generate axially symmetric diffusion parameters from the local overall correlation times. Table 3 contains the rotational diffusion parameters obtained from the model-free results. Both structures yield axially symmetric diffusion tensors consistent with an oblate object, which is hardly surprising considering the shape of the cyclic carbohydrate molecule. From the square structure $D_\parallel/D_\perp = 0.75$ is obtained, and the rhombic structure yields $D_\parallel/D_\perp = 0.72$. The results using the rhombic structure are slightly better than from using the square structure ($\chi^2 = 61$ vs. $\chi^2 = 71$). As shown by F statistics, there is a significant improvement in both cases when using the axially symmetric model ($F = 10.2$ for the rhombic structure and $F = 6.7$ for the square structure). A slight improvement in the fit is obtained by using a totally asymmetric diffusion tensor ($\chi^2 = 55$ for the rhombic structure and $\chi^2 = 64$ for the square structure), but the F-test shows that the improvement is not statistically significant.

The values for the principal components of the moment of inertia tensor can be used to estimate the rotational diffusion anisotropy, where $I_\perp = (I_{xx} + I_{yy})/2$ and $I_\parallel = I_{zz}$. Assuming axial symmetry, the anisotropy can be estimated from $D_\parallel/D_\perp \approx (I_\perp/I_\parallel)^{0.7}$ (Copié et al., 1998), and for cECA the $D_\parallel/D_\perp$ ratio becomes 0.65 for both the rhombic and square structures. This agrees well with the experimentally obtained value of 0.72 for the rhombic structure. As has previously been discussed (Rundlöf et al., 1999), calculation of the diffusion anisotropy from the moment of inertia tensor is generally overestimated, as is also the case here. Nevertheless, the agreement gives confidence in the analysis of the rotational correlation times for cECA in terms of an axially symmetric diffusion model.

The results of the model-free fitting also provide the parameters describing the local mobility of each C–H spin vector within the rings (Table 2). The local dynamics of cECA are seen to be slightly residue dependent. The mean values of S^2 for the three residues are 0.79 ± 0.04 for the F residue, 0.71 ± 0.03 for the M residue and 0.77 ± 0.02 for the G residue. The local correlation times are in the range of 46–161 ps, which is somewhat slower than what is typically found for oligosaccharides (Kowalewski and Widmalm, 1994; Mäler et al., 1995, 1996a, b; Kjellberg et al., 1998; Rundlöf et al., 1999). Again, a difference between the residues is observed with a mean value of τ_e of 83 ± 18 ps for the F residue, 107 ± 48 for the M residue, and 85 ± 41 ps for the G residue. The spread in correlation times within the residues is however large, but nevertheless, the difference in both order parameters and local correlation times clearly indicate residue specific local dynamics.

Discussion

The cyclic form of ECA has been shown to crystallize into two distinct forms, a square and a rhombic structure (see Figure 2). There is a two-fold symmetry axis in the structures, which makes two of the four repeats identical. Thus, there are six structurally different residues in cECA. In solution there is no evidence for the existence of two structural variants of the carbohydrate, nor of differences between the repeats. The NMR spectrum shows one set of signals, but fast exchange between two conformers cannot be excluded. Analysis of in particular field-dependent R_2 relaxation data can provide insights into exchange phenomena, as chemical exchange scales with the square of the magnetic field strength. In the present analysis we see no evidence of exchange, since a phenomenological exchange rate R_{ex} was not needed to explain the multiple-field carbon-13 relaxation data.

A complex carbohydrate such as the present cECA may not be expected to undergo isotropic global rotational diffusion. In previous studies of smaller oligosaccharides, the concept of "dynamical equivalence" has been used (Kowalewski and Widmalm, 1994; Mäler et al., 1995). This term refers to cases where all ^{13}C–^{1}H vectors within a sugar residue are seen to undergo similar dynamics. This is usually seen already in comparing the input relaxation rates, and in cases when the relaxation rates are equal for all sites, average values for the entire residue have been used. In cECA the relaxation rates are seen to differ somewhat within each residue (Table 1), and one may not speak of "dynamical equivalence". Therefore the dynamics were evaluated separately for each site. This analysis ultimately yielded an axially symmetric global rotational diffusion, with parameters listed in Table 3. It can clearly be seen

Table 2. Motional parameters obtained from modelfree analysis, using Equation 4, of ^{13}C relaxation data for the ring carbons of cECA using a local global correlation time for each site

Carbon[a]	τ_{loc} (ns)	S^2	τ_e (ps)
F–C1	2.16 ± 0.09	0.82 ± 0.03	108 ± 37
F–C2	2.27 ± 0.10	0.70 ± 0.03	84 ± 17
F–C4	2.03 ± 0.08	0.81 ± 0.03	67 ± 26
F–C5	2.17 ± 0.08	0.80 ± 0.02	73 ± 12
M–C1	2.13 ± 0.12	0.68 ± 0.03	118 ± 24
M–C2	2.43 ± 0.11	0.74 ± 0.03	141 ± 31
M–C3	1.86 ± 0.09	0.67 ± 0.03	71 ± 16
M–C4	2.27 ± 0.12	0.74 ± 0.04	161 ± 41
M–C5	1.89 ± 0.09	0.73 ± 0.03	46 ± 17
G–C1	2.00 ± 0.08	0.80 ± 0.02	70 ± 12
G–C2	2.06 ± 0.10	0.76 ± 0.03	105 ± 25
G–C3	1.94 ± 0.09	0.78 ± 0.03	59 ± 23
G–C4	2.15 ± 0.10	0.76 ± 0.03	146 ± 37
G–C5	2.02 ± 0.09	0.75 ± 0.03	44 ± 17

[a]Relaxation parameters were not measured for F–C3.

that the molecule has an oblate symmetry with $D_{\|}/D_{\perp}$ of 0.72 (rhombic structure) or 0.75 (square structure). It should be emphasized that although the differences in relaxation parameters within each residue are not pronounced, a careful analysis yields a clear asymmetry in the rotational diffusion. This is important, since many times small differences in relaxation parameters may be overlooked, resulting in erroneous interpretation of relaxation data. Much attention has been devoted to investigating local dynamics in carbohydrates (Bagley et al., 1992; Kowalewski and Widmalm, 1994; Mäler et al., 1995, 1996a, b; Poveda et al., 1997a, b; Kjellberg et al., 1998; Lippens et al., 1998; Lycknert and Widmalm, 2004), and a few reports have also included anisotropic overall tumbling in oligosaccharides (Ejchart and Dabrowski, 1992; Hricovíni and Torri, 1995; Hricovíni et al., 1995; Rundlöf et al., 1999). It is clear that neglecting possible rotational anisotropy may result in overestimating the influence of local dynamics, as well as erroneous interpretation of for instance contributions from chemical exchange. It is useful to compare the axially symmetric diffusion tensor with the hydrodynamic description in solution. Figure 5 shows an overlay of the moment of inertia tensor with the axially symmetric diffusion tensor. The results are slightly better for the rhombic structure, and one can clearly see that the calculated moment of inertia tensor agrees very well with the axially symmetric diffusion model (Figure 5).

Turning to the local motion in cECA, we see similar order parameters to what is typically found for carbohydrates, but longer local correlation times. This may be due to the fact that cECA is a larger oligosaccharide than those previously investigated in our laboratory (Bagley et al., 1992; Kowalewski and Widmalm, 1994; Mäler et al., 1995, 1996a, b; Kjellberg, et al., 1998; Rundlöf

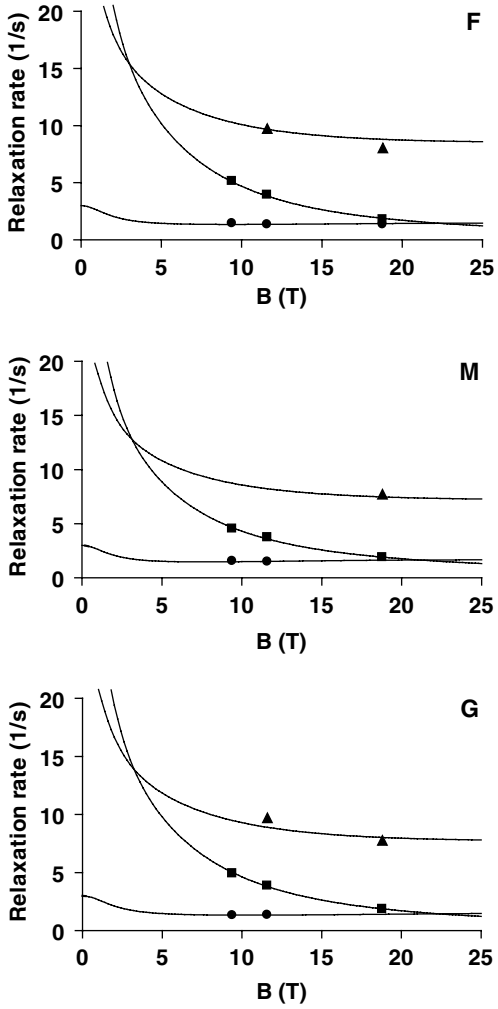

Figure 4. Relaxation data for the C1 carbons in cECA. Experimentally determined R_1 values are depicted as squares, R_2 values are shown as triangles and NOE-factors are shown as circles. The solid lines indicate theoretically calculated values for the relaxation rates obtained using motional parameters from Table 2. The top panel shows relaxation rates for the F residue, the middle panel for the M residue, and the lower panel shows the relaxation rates for the G residue.

Table 3. Rotational diffusion analysis of ring carbons in cECA using two different crystal structures[a]

	Isotropic model		Axially symmetric model				
Structure	$D_{iso}(10^{-7}\ s^{-1})$	χ^2	$D_{iso}(10^{-7}\ s^{-1})$	$D_{\|}/D_{\perp}$	θ (deg)	ϕ (deg)	χ^2
Square	7.76 ± 0.05	100	7.57 ± 0.07	0.75 ± 0.04	80 ± 4	−1 ± 4	71
Rhomb	7.76 ± 0.05	100	7.54 ± 0.06	0.72 ± 0.04	90 ± 4	0 ± 4	61

[a]All sites in cECA except F–C3 were used, resulting in 56 distinct CH vectors in the structure.

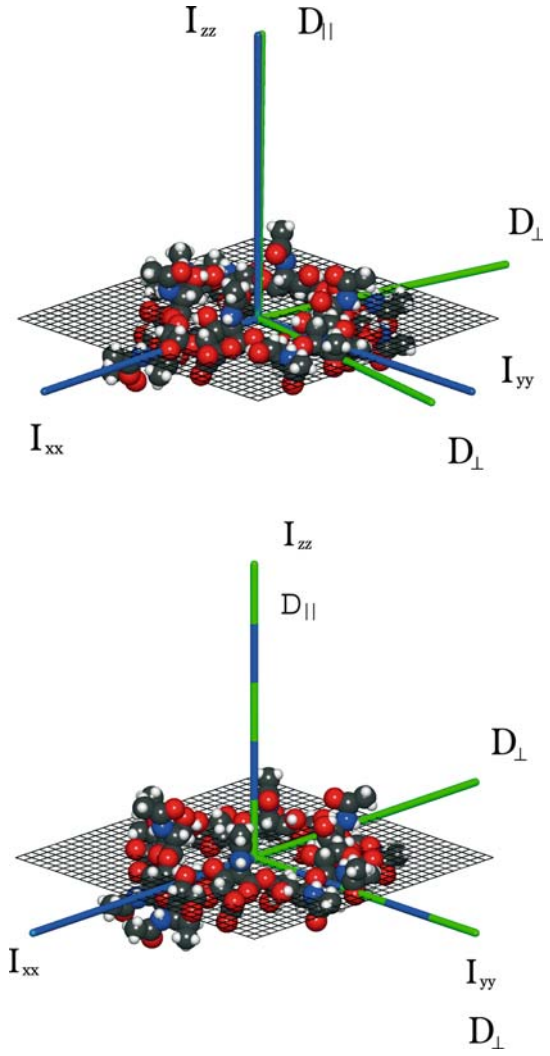

Figure 5. The principal axes of the moment of inertia tensor, and the principal axes of the axially symmetric diffusion tensor of cECA shown on the two crystal forms of ECA. The top panel shows the square form of cECA and the lower panel the rhombic form of cECA. The principal components of the inertia tensor are labeled with I_{zz}, I_{yy} and I_{xx}, where $I_{zz} > I_{yy} > I_{xx}$ and are shown in blue. The principal components of the axially symmetric diffusion tensor, $D_{\|} = D_{zz}$,$D_{\perp} = D_{xx} = D_{yy}$, where $D_{\|} < D_{\perp}$, are shown in green.

et al., 1999), but may also be a reflection of including motional anisotropy in the present analysis. When examining the order parameters a significant difference can be seen between the residues. The central M residue in the repeat unit (Figure 1) has on average lower order parameters than the F and G residues (Table 2). In a previous study of cECA (Staaf et al., 2001) molecular dynamics simulations showed that there is a possibility that the M residue undergoes conformational exchange, as it was seen that two distinct pairs of torsional angle values were possible. It is interesting to relate this observation with the present results on the differences in local dynamics. If the conformational exchange is very fast, it may in fact manifest itself as increased local mobility, which agrees very well with the observation of somewhat lower order parameters, and differences in local correlation times as compared to the F and G residues. It is tempting to speculate in terms of exchange between the two forms of the structure present in the solid state, but this seems to involve a much more complicated exchange process. Instead, the difference in local mobility is most likely related to the possibility of the M residues to undergo a torsional motion, while the two end residues are more rigid.

Dynamical investigations of carbohydrates have attracted considerable attention, especially concerning the rigidity of the glycosidic linkages. Here we see a clear difference in order parameters for in particular the C1 carbons, with $S^2 = 0.82$ for F–C1, $S^2 = 0.80$ for G–C1 and $S^2 = 0.68$ for M–C1. One may note that the M–C1 is connected to the G residue through a β-glycosidic linkage, while the two other are α-linkages. This may indeed be related to local flexibility, but an interpretation based solely on the configuration difference at the anomeric position is too simplistic. A study of the conformational flexibility of α- vs. β-linkages investigated for disaccharides did not reveal any significant difference when interpreted by the model-free approach (Söderman and Widmalm, 1999).

In summary, we have analyzed multiple-field carbon-13 relaxation data in terms of an axially symmetric diffusion with local motion. The results clearly show the need for careful analysis of relaxation data in terms of rotational anisotropy. With this analysis we were able to identify differences in local mobility between the residues, which may be related to differences in the glycosidic linkages and to the structural position of the central M residue. In the present investigations we see no evidence of fast exchange between conformers, but still find that the solid-state structure of cECA, consisting of two distinct structural forms, fits well with the relaxation data. Likewise, translational diffusion and hydrodynamical considerations confirm the results on the global motional properties of the molecule.

The enterobacterial common antigen has been shown to be important for *E. coli* in its resistance to organic acids (Barua et al., 2002). With the structure and conformational dynamics determined for cECA, it should be possible in future investigations to identify the role of this cyclic oligosaccharide produced by bacteria of the genus Enterobacteriaceae.

Acknowledgement

This work was supported by grants from the Swedish Research Council.

References

Aue, W.P. Bartholdi, E. and Ernst, R.R. (1976) *J. Chem. Phys.*, **64**, 2229–2246.

Bagley, S. Kovacs, H. Kowalewski, J. and Widmalm, G. (1992) *Magn. Reson. Chem.*, **30**, 733–739.

Barua, S. Yamashino, T. Hasegawa, T. Yokoyama, K. Torii, K. and Ohta, M. (2002) *Mol. Microbiol.*, **43**, 629–640.

Beveridge, T.J. (1999) *J. Bacteriol.*, **181**, 4725–4733.

Braunschweiler, L. and Ernst, R.R. (1983) *J. Magn. Reson.*, **53**, 535–360.

Brüschweiler, R. Lia, X. and Wright, P. (1995) *Science*, **268**, 886–889.

Callaghan, P.T. Komlosh, M.E. and Nydén, M. (1998) *J. Magn. Reson.*, **133**, 177–182.

Cantor, C.R. and Shimmel, P.R. (1980) *Biophysical chemistryPart II, Techniques for the study of biological structure and function*, W.H. Freeman and company, San Francisco.

Cavanagh, J. Fairbrother, W.J. Palmer, A.G. and Skelton, N.J. (1996) *Protein NMR Spectroscopy*Academic Press, San Diego.

Chou, J.J. Baber, J.L. and Bax, A. (2004) *J. Biomol. NMR*, **29**, 299–308.

Clore, G.M. Szabo, A. Bax, A. Kay, L.E. Driscoll, P.C. and Gronenborn, A. (1990) *J. Am. Chem. Soc.*, **112**, 4989–4991.

Copié, V. Tomita, Y. Akiyama, S.K. Aota, S.-I. Yamada, K.M. Venable, R.M. Pastor, R.W. Krueger, S. Torchia, D.A. (1998) *J. Mol. Biol.*, **277**, 663–682.

Damberg, P. Jarvet, J. and Gräslund, A. (2001) *J. Magn. Reson.*, **148**, 343–348.

Ejchart, A. and Dabrowski, J. (1992) *Magn. Reson. Chem.*, **30**, S115–S124.

Erbel, P.J.A. Barr, K. Gao, N. Gerwig, G.J. Rick, P.D. and Gardner, K.H. (2003) *J. Bacteriol.*, **185**, 1995–2004.

Erbel, P.J.A. Seidel, R. Macintosh, S.E. Gentile, L.N. Amor, J.C. Kahn, R.A. Prestegard, J.H. McIntosh, L.P. and Gardner, K.H. (2004) *J. Biomol. NMR*, **29**, 199–204.

Färnbäck, M. Eriksson, L. Senchenkova, S. Zych, K. Knirel, Y.A. Sidorczyk, Z. and Widmalm, G. (2003) *Angew. Chem. Int. Ed.*, **42**, 2543–2546.

Hricovíni, M. and Torri, G. (1995) *Carbohydr. Res.*, **268**, 159–175.

Hricovíni, M. Guerrini, M. Torri, G. Piani, S. and Ungarelli, F. (1995) *Carbohydr. Res.*, **277**, 11–23.

Hwang, T.-L. and Shaka, A.J. (1995) *J. Magn. Reson. A*, **112**, 275–279.

Jeener, J. Meier, B.H. Bachmann, P. and Ernst, R.R. (1979) *J. Chem. Phys.*, **71**, 4546–4553.

Karlsson, C. Jansson, P.-E. and Skov Sørensen, U.B. (1999) *Eur. J. Biochem.*, **265**, 1091–1097.

Kjellberg, A. Rundlöf, T. Kowalewski, J. and Widmalm, G. (1998) *J. Phys. Chem. B*, **102**, 1013–1020.

Kuhn, H.-M. Meier-Dieter, U. and Mayer, H. (1988) *FEMS Microbiol. Rev.*, **54**, 195–222.

Lee, L.K. Rance, M. Chazin, W.J. and Palmer, A.G. III (1997) *J. Biomol. NMR*, **9**, 287–198.

Lipari, G. and Szabo, A. (1982) *J. Am. Chem. Soc.*, **104**, 4546–4559.

Lippens, G. Wieruszkski, J.-M. Horvath, D. Talaga, P. and Bohin, J.-P. (1998) *J. Am. Chem. Soc.*, **120**, 170–177.

Lycknert, K. and Widmalm, G. (2004) *Biomacromolecules*, **5**, 1015–1020.

Mandel, A.M. Akke, M. and Palmer, A.G. (1995) *J. Mol. Biol.*, **246**, 144–163.

Mäler, L. Lang, J. Widmalm, G. and Kowalewski, J. (1995) *Magn. Reson. Chem.*, **33**, 541–548.

Mäler, L. Widmalm, G. and Kowalewski, J. (1996a) *J. Biomol. NMR*, **7**, 1–7.

Mäler, L. Widmalm, G. and Kowalewski, J. (1996b) *J. Phys. Chem.*, **100**, 17103–17110.

Palmer, A.G. Rance, M. and Wright, P.E. (1991) *J. Am. Chem. Soc.*, **113**, 4371–4380.

Phan, I.Q.H. Boyd, J. and Campbell, I.D. (1996) *J. Biomol. NMR*, **8**, 369–378.

Poveda, A. Santamaria, M. Bernabe, M. RiveraA. Corzo, J. and Jiménez-Barbero, J. (1997a) *Carbohydr. Res.*, **304**, 219–228.

Poveda, A. Asensio, J.L. Martín-Pastor, M. and Jiménez-Barbero, J. (1997b) *J. Biomol. NMR*, **10**, 29–43.

Rundlöf, T. Venable, R.M. Pastor, R.W. Kowalewski, J. and Widmalm, G. (1999) *J. Am. Chem. Soc.*, **121**, 11847–11854.

Skelton, N. Palmer, A.G. Akke, M. Kördel, J. Rance, M. and Chazin, W.J. (1993) *J. Magn. Reson. B*, **102**, 253–264.

Söderman, P. and Widmalm, G. (1999) *Magn. Reson. Chem.*, **37**, 586–590.

Staaf, M. Höög, C. Stevensson, B. Maliniak, A. and Widmalm, G. (2001) *Biochemistry*, **40**, 3623–3628.

Stejskal, E.O. and Tanner, J.E. (1965) *J. Phys. Chem.*, **42**, 288–292.

Vinogradov, E.V. Knirel, Y.A. Thomas-Oates, J.E. Shashkov, A.S. and L'vov, V.L. (1994) *Carbohydr. Res.*, **258**, 223–232.

von Meerwall, E. and Kamat, M. (1989) *J. Magn. Reson.*, **83**, 309–323.

Wei, Y. Lee, D.-K. and Ramamoorthy, A. (2001) *J. Am. Chem. Soc.*, **123**, 6118–6126.

Woessner, D.E. (1962) *J. Chem. Phys.*, **27**, 647–654.